33RD CONGRESS
OF THE INTERNATIONAL COUNCIL
OF THE AERONAUTICAL SCIENCES
STOCKHOLM, SWEDEN, 4-9 SEPTEMBER, 2022

ICAS 2022 SWEDEN

# ANALYSIS OF THE HAMMERHEAD LAUNCH VEHICLE USING CFD-CAE COUPLED METHOD IN THE TRANSONIC REGION

Hong-gi Rho[1], Phuc Anh Nguyen[1], Jae-sung Bae[1], Soo-hyung Park[2], Kwan-Hwa Byun[3]

[1]Department of Aerospace and Mechanical Engineering, Korea Aerospace University
[2]Department of Aerospace Information Engineering, Konkuk University
[3]Korea Agency for Defense Development

## Abstract

An aeroelastic stability analysis of the hammerhead launch vehicle using computational fluid dynamics (CFD) and computational aeroelasticity (CAE) coupled method in transonic region is performed to predict the aeroelastic phenomena such as flutter, divergence and buffet. Time domain analysis was performed by a coupled time-integration method in which implicit time schemes for CFD and explicit time schemes for CAE are loosely coupled. Frequency-domain analyses with harmonic oscillation method are performed using V-g & p-k methods. Beam spline method has been used for displacements and aerodynamic forces interpolations between CFD mesh and FEM model. In order to verify the obtained results, the comparison and verification were carried out on the launch vehicle. The obtained results shown that divergence could occur in the worst case of the launch vehicle.

**Keywords:** Aeroelasticity, Flutter, CFD-CAE coupling, Transonic region, Launch Vehicle

## 1. Introduction

The modern large launch vehicle consists of a first stage rocket, a second stage rocket, and a third stage rocket connected to the payload. The three-stage payload is covered with a pairing to protect air flow and heat, and there are various types of pairing depending on the type of payload. When the size of the payload is larger than the diameter of the launch vehicle, a hammerhead-shaped pairing is used for nose pairing. A launch vehicle having a hammerhead-type nose pairing can generates a complex type of shock wave and flow near the pairing. This is caused by the change in the launch vehicle's cross-sectional area in the axial direction. In the transonic region, it has a more complex flow due to normal shock waves and flow separation. In the transonic region, the flow is accelerated around the pairing to become supersonic, and normal shock waves is generated near the neck where the hammerhead-shaped pairing and the launch vehicle meet. In addition, the boundary layer generated from the nose is further expanded by flow separation generated near the neck of the hammer head. A recirculation region of the expansion part is generated due to interference between the normal shock wave and the flow separation near the neck, and thus, a more complicated pressure vibration phenomenon occurs, which causes aeroelastic phenomena of the launch vehicle. Since the development of Saturn I, aeroelasticity stability has received continuous attention [1,2]. The hammerhead shaped launch vehicle had potential aeroelastic instability, and experimental analytical studies were performed in the United States [3,4].

Rainey [5] of NASA LRC described the development of the Apollo-Saturn rocket as a study of buffet phenomenon. Reding and Ericsson [6] of Lockheed Missiles & Space Company performed a study on the aeroelastic stability of launch vehicle with hammerhead-type nose pairing. Dotson et al. [7~9] of Aerospace Corp. proposed nonlinear response analysis and aeroelastic stability analysis techniques of launch vehicle buffets in consideration of aeroelastic coupling term.

Robert C. et al [10]. studied the effect of the angle and diameter of the boattail on the unsteady aerodynamic forces of the hammerhead launch vehicle through a wind tunnel test. It was confirmed

that unsteady aerodynamic forces became instable due to vibration from the buffet phenomenon caused by flow separation.

Perry W. Hanson and Robert V. Doggett [11,12] studied the aerodynamic damping and buffet response at Mach 0.8 and 1.2. The effects of aerodynamic damping and bending moment were investigated with an Apollo launch vehicle model with payload, and the results of the full-scale experiment data and the buffet response were compared with theoretical results.

In recent years, Mastroddi et al [13]. performed linearized aeroelastic analysis of launch vehicle in the transonic region using Computational Fluid Dynamics (CFD). Barteled [14] of NASA LRC performed an aeroelastic analysis of the Ares launch vehicle using CFD and compared it with the analysis results with CFD-Computational Aeroelasticity (CAE).

In this study, an analytical study was performed to predict aeroelastic phenomena such as flutter, divergence and buffet that may occur during the flight of a hammerhead launch vehicle. The following two methods are used. The first method is considering aeroelastic coupling term. It is a method of calculating unsteady aerodynamic forces on the axial bending deformation of a launch vehicle using CFD, and applying it to an aeroelastic equation to perform aeroelastic analysis in frequency and time domain. The second method is CFD-CAE coupling method. The aeroelastic response is obtained by CFD-CAE coupled analysis, and the aeroelastic stability of the launch vehicle is determined.

In this study, the in-house CFD code KFLOW was used for CFD analysis. The MSC.NASTRAN program was used for FEM analysis. Time-domain analyses by CFD-CAE coupling method have been performed. In this CFD-CAE coupling method, the implicit temporal scheme for CFD and explicit temporal scheme for CAE are loosely coupled. The Hormonic Oscillation Method (HOM) was used to calculate the unsteady aerodynamic force coefficient (UAIC) in the frequency domain. The beam spline method was used as the numerical interpolation between the CFD mesh and the FEM model. For the aeroelastic analysis, the V-g and p-k methods were used for the frequency domain analysis, and the time-matching method was used for the time domain analysis. The Karpel's minimum-state approximation (MSA) method was used for unsteady aerodynamic force approximation.

## 2. CFD Analysis of the Hammerhead Launch Vehicle

### 2.1 Steady Aerodynamic Force Verification

Technical Memo.X-778 experimental data from Coe and Nute [15] were used to verify the computational fluid analysis program KFLOW. Coe measured the average pressure $C_{p,mean}$ and the second order average pressure $C_{p,r.m.s}$ using unsteady pressure for each angle of attack at the Mach number 0.6 to 1.17 for Model 11 with hammerhead nose pairing as shown in Figure 1. The Model 11 has a boattail shape of more than 31 degrees after two expansion corners.

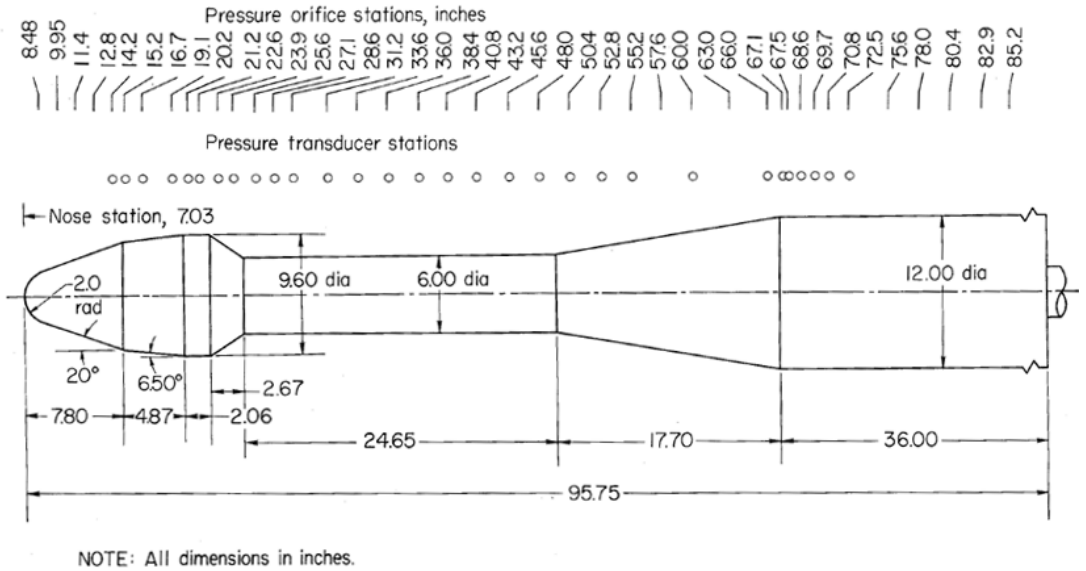


Figure 1 - Schematic shape of Model 11 used in Coe's experiment [15].

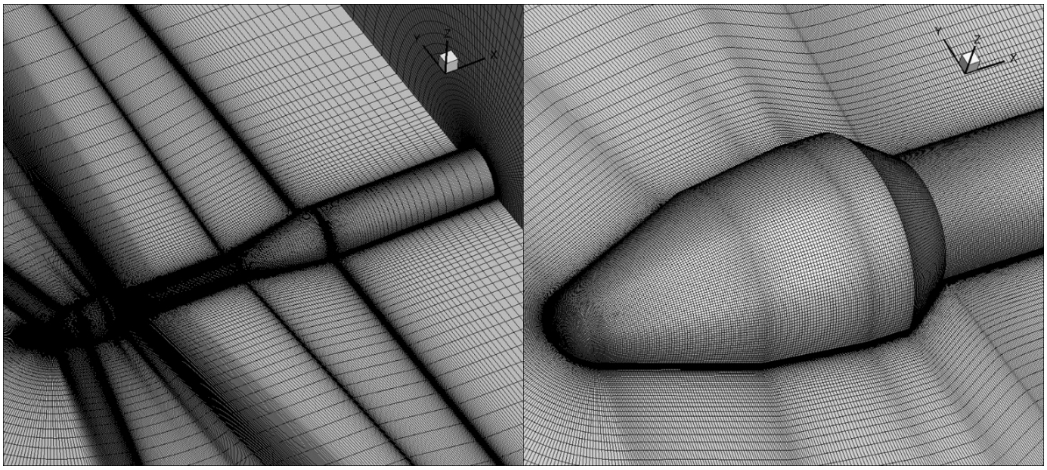

Figure 2 – CFD mesh of Model 11

Figure 2 shows the CFD mesh used in this analysis. The CFD mesh has a distance of $5.0\times10^{-5}$ from the wall to the first cell, and the total number of grids is 521×129×121. The entire grid was interpreted by giving symmetric boundary conditions, and Riemann's invariant inflow and outflow boundary conditions were applied at Mach 0.81, and in the case of Mach 1.17, supersonic inflow and outflow boundary conditions were applied. The y-plus number represents a dimensionless distance from the wall boundary in consideration the Reynolds number was 1.0 or less. Considering that the wind tunnel used in the experiment by Coe was a closed circulation wind tunnel, the adiabatic wall boundary conditions were used with the assumption that the wall temperature conditions converged. The turbulence model used was the S-A one equation model, CFL number was 1.0, Roe scheme was used as the spatial discretization method, and 3rd order MUSCL was used to obtain a higher order solution.

| Parameter | Value |
|---|---|
| Re. number | $1.3123\text{x}10^{7}$ |
| M | 0.81, 1.17 |
| Mesh | 521×129×101 |
| First cell distance | $5.0\times10^{-5}$ |
| Turbulent model | S-A one equation model |
| CFL number | 1.0 |
| Flux scheme | Roe scheme |
| Limiter | 3rd order MUSCL |

Table 1 – CFD Conditions for Steady Analysis

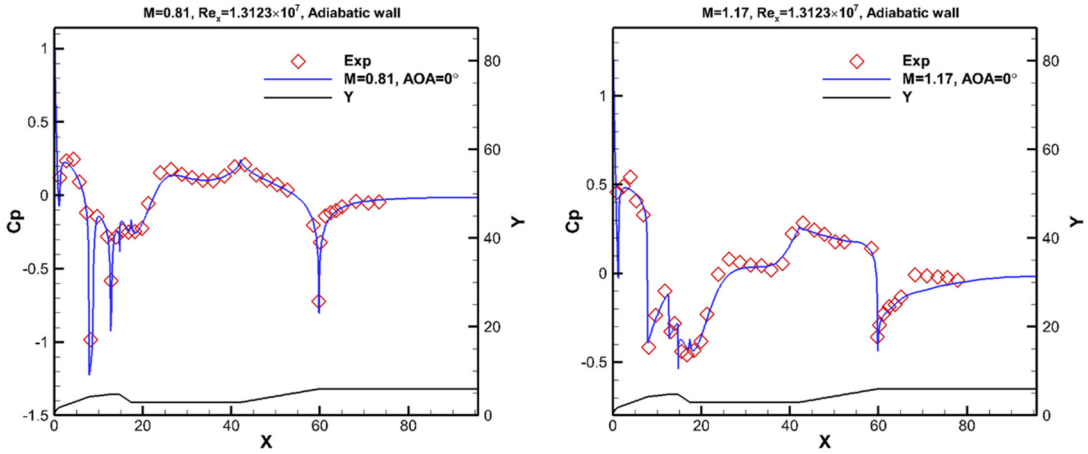


Figure 3 - Comparison of pressure coefficients with experiments at M = 0.81 and 1.71 , AOA = 0°

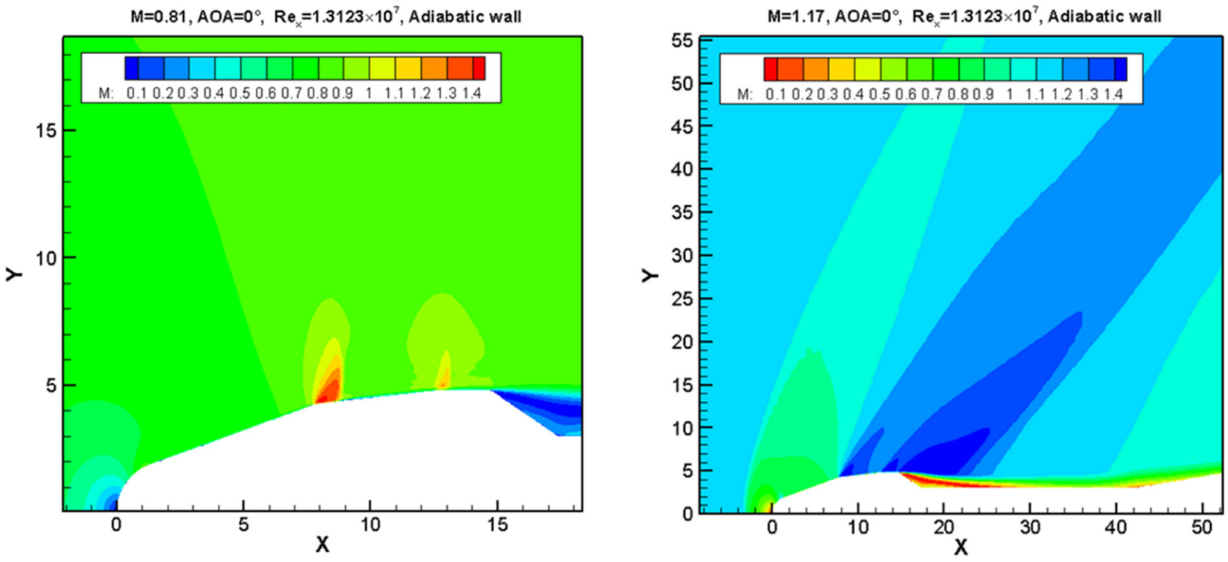


Figure 4 – Mach Contour at M = 0.81 and 1.71, AOA = 0°

Figure 3 shows the comparison of the CFD steady analysis result of KFLOW and the experimental data of Coe. It shows that the pressure coefficients match very well in the two different Mach numbers. Figure 4 shows the Mach contour at two different Mach numbers. In case of the Mach No. is 0.81, it was predicted that the flow would be accelerated to supersonic speed when passing through the expansion corner after the pressure increased at the stagnation point of the nose, and normal shock waves would be generated on the launch vehicle. In case of the Mach No is 1.71, the Bow shock waves occur before the stagnation point of the nose, and oblique shock waves occur as they pass through the expansion corner.

## 2.2 Unsteady Aerodynamic Force Verification

In the shape of Model 11, a large recirculation area exists due to a change in a cross-sectional area in the expansion corner of the boattail. To simulate the unsteady aerodynamic force caused by this, the results of each 2D axisymmetric Unsteady RANS, Delayed DES (DDES), and 3D DDES were compared and verified with Coe's experimental data, from the time-averaged pressure coefficient and pressure vibration. The time-average pressure was simply calculated as the first average of the pressure, and the pressure vibration was calculated as the secondary average of the difference between the pressure and the average pressure over time as follows.

$$\bar{C_p} = \frac{1}{T}\int_0^T C_p \, dt \tag{1}$$

$$C_{p,R.M.S} = \sqrt{\frac{1}{T}\int_0^T \left(C_p - \bar{C_p}\right)^2 dt} \tag{2}$$

As in the steady analysis, the grid in Figure 2 was used. In order to reduce the unsteady calculation time, the grid was composed of 1/4 and the effect by the angle of attack were excluded. The total number of grids is 521×129×51. The 5$^{th}$ order TVD limiter is used. The pseudo CFL number of the dual time stepping method was 1.0. Other conditions are the same as steady analysis and Mach No. is 0.81.

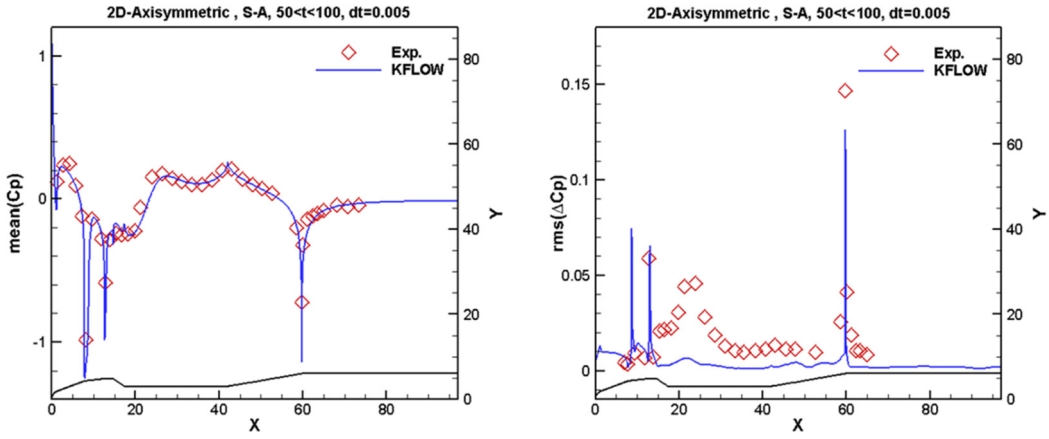


Figure 5 – 2D, S-A, URANS

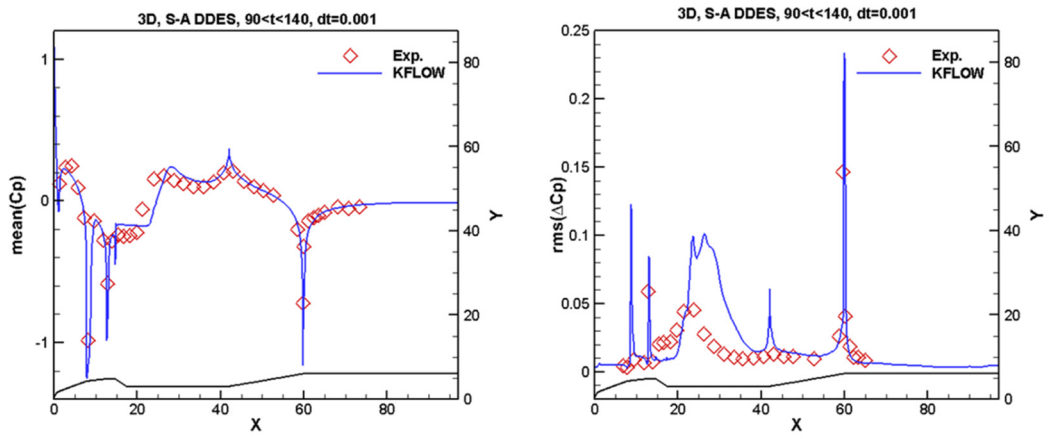


Figure 6 – 3D, S-A, DDES

Figure 5 and Fig. 6 show both 2D, S-A, RANS and 3D, S-A, DDES showed a pressure coefficient distribution similar to the experimental values. However, pressure vibration is larger than the experimental value which was predicted in the recirculation area. Murman et al [16]. explained that the turbulent shear stress of the separated shear layer was calculated to be lower than the actual flow because the pressure vibration of the recirculation region tends to be excessively measured the results of SST DDES and S-A DDES. The calculation results of this study also showed similar results.

## 3. Aeroelasticity Stability Analysis of the Hammerhead Launch Vehicle

### 3.1 Beam Spline Method and Harmonic Oscillation Method

#### *3.1.1 Beam Spline Method*

The aeroelasticity deals with the problem of simultaneous consideration of fluid and structure. However, CFD models and FEM models perform analysis by selecting different coordinate systems to increase computational efficiency. As a result of this, there is a big difference between the FEM model and the CFD mesh. The fluid and the structural mesh can be connected by various numerical interpolation methods such as an Infinite-plate Spline method, Thin-plate Spline method and Beam spline method. In this study, the Beam Spline Method was used. The Beam Spline Method is a one-dimensional linear interpolation numerical technique that has a theoretical background in the equation of infinite beams. The Beam Spline method can obtain torsion and deformation for each direction of Euler beam using mode shape in each structural grid of an actual model using a virtual infinite beam element crossing the elastic axis. It is mainly used for the fuselage surface splines of aircraft and launch vehicle.

### *3.1.2 Harmonic Oscillation Method*

The Harmonic Oscillation Method (HOM) is a method of calculating the Unsteady Aerodynamic Influence Coefficient (UAIC) in the frequency domain by forced vibrating the CFD mesh with the shape of the natural mode shape of the FEM model with the reduced frequencies.

The CFD mesh is forced vibrated with the $j^{th}$ natural mode shape for some reduced frequencies. A continuous unsteady aerodynamic response in the time domain is obtained, and in this case, the UAIC for all $i^{th}$ structural modes is calculated. The real and imaginary part of unsteady aerodynamic forces in the frequency domain can be calculated as follows equations.

$$Re\left[A_{ij}(M,k)\right] = -\left(\frac{A_{ij}\left(\frac{3}{2}\pi\right) - A_{ij}\left(\frac{1}{2}\pi\right)}{2\times Amplitude}\right) \tag{3}$$

$$Im\left[A_{ij}(M,k)\right] = -\left(\frac{A_{ij}(\pi) - A_{ij}(2\pi)}{2\times Amplitude}\right) \tag{4}$$

## 3.2 Aeroelasticity Stability Analysis

### *3.2.1 Analysis Model*

The aeroelasticity stability analysis was performed by referring to KSLV II, the hammerhead model of the Korea Aerospace Research Institute. From the provided data, a FEM model with an appropriate mass and stiffness distribution with a low natural frequency was designed. Figures 7 -9 show FEM model with beam elements, the mass and stiffness distributions, and first four natural frequencies and mode shapes, respectively.

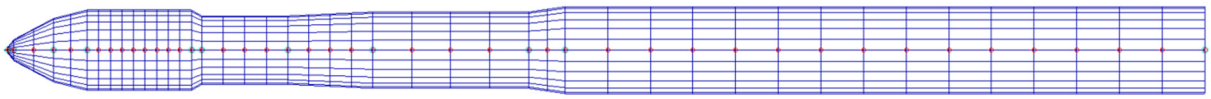

Figure 7 – FEM model of KSLV II

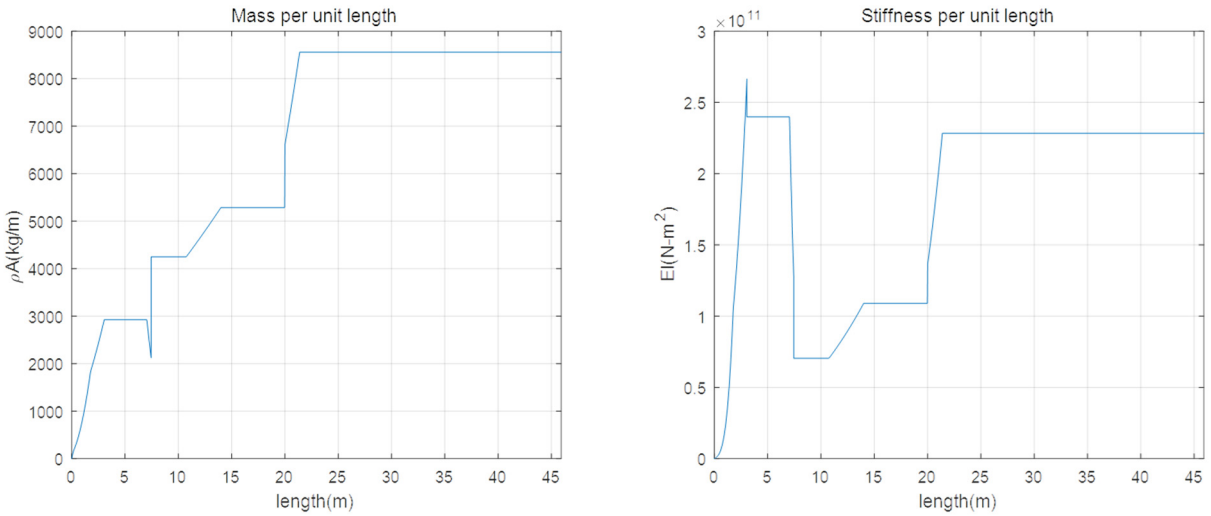


Figure 8 – Mass and Stiffness distribution of KSLV II

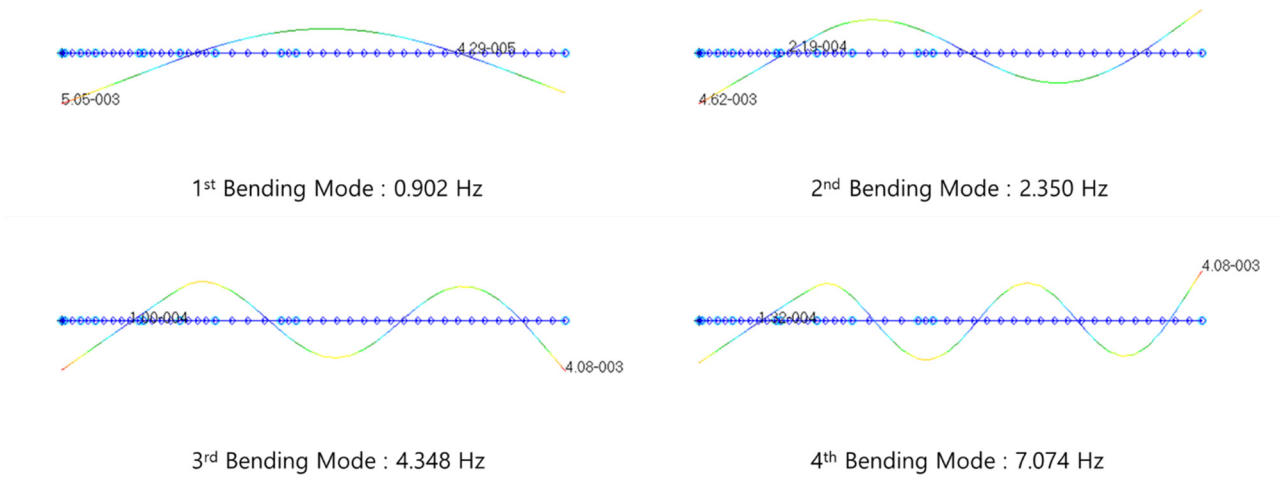


Figure 9 – Normal mode shapes and natural frequencies of KSLV II

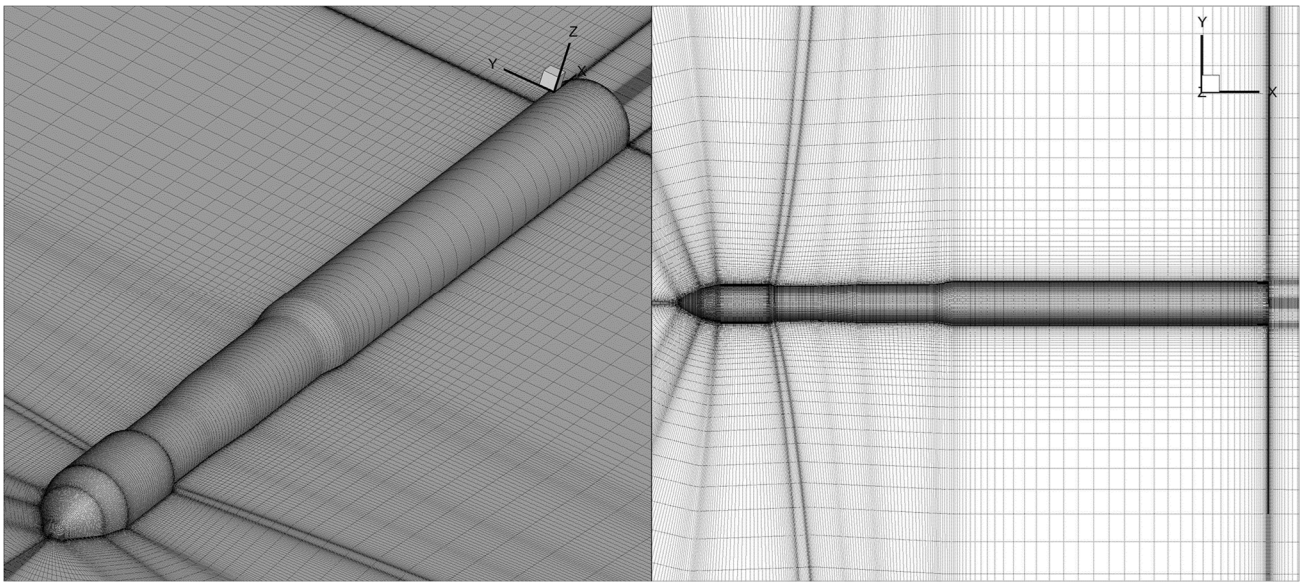


Figure 10 – CFD mesh of KSLV II

The CFD mesh consists of two sub-blocks to avoid singularity point at the nose of the launch vehicle, and each of sub-blocks have 25x81x13 and 49x81x325 nodes in i, j, and k directions, respectively. The CFD mesh is shown in Fig. 10. Figure 11 shows pressure coefficient contour and Mach filed contour at Mach number of 0.88 and angle of attack of 0°. It shows that the normal shock wave and the recirculation region are predicted almost similar to those showed in Figure 4.

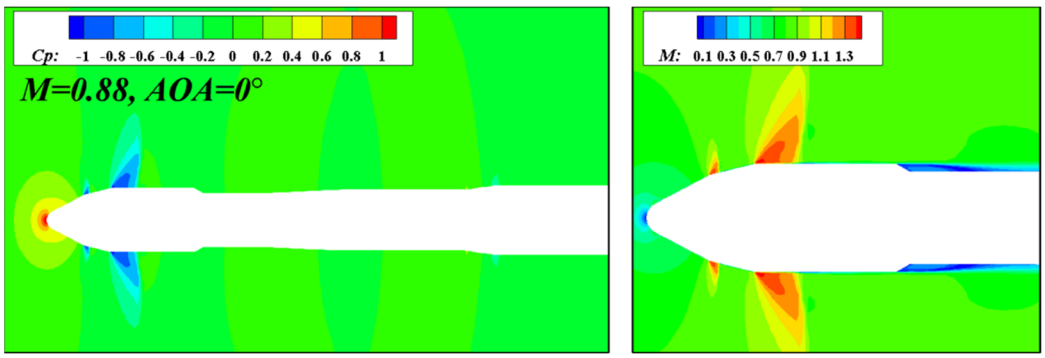


Figure 11 – Cp and Mach field contours at M = 0.88 and AOA = 0°

### *3.2.2 Frequency Domain Analysis*

Mach number used in this analysis was 0.88, and eight reduced frequencies values between 0 and 1 were selected. The program was developed so that the steady flow analysis was pre-performed by the input Mach number, and then the launch vehicle vibrated according to the input frequency, and the modal displacement and force at the modal coordinate system were output in a dimensionless time domain. Figure 11 shows the unsteady aerodynamic force response in the modal coordinate system when the CFD grid is forced vibrated by 3 cycles with 0.2 reduced frequency.

It was confirmed that the response was stable from the third cycle, and unsteady aerodynamic force at the frequency domain was calculated using last cycle.

Analysis was repeatedly performed in the same way for four modes and eight reduced frequencies, and the UAIC matrix was calculated. Figure 11 shows the results of $A_{11}$ to $A_{22}$ in the UAIC matrix.

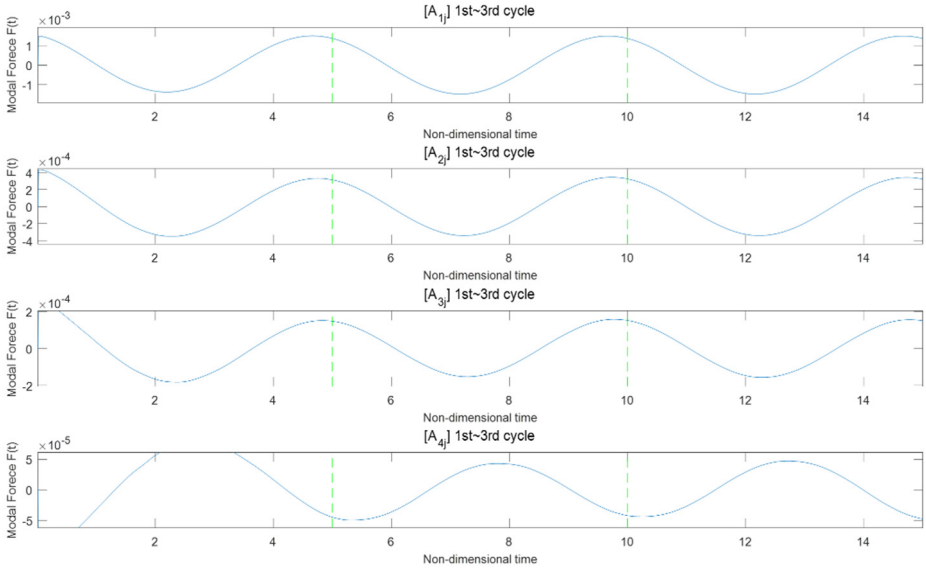


Figure 12 – Time history of unsteady aerodynamic force at modal coordinate

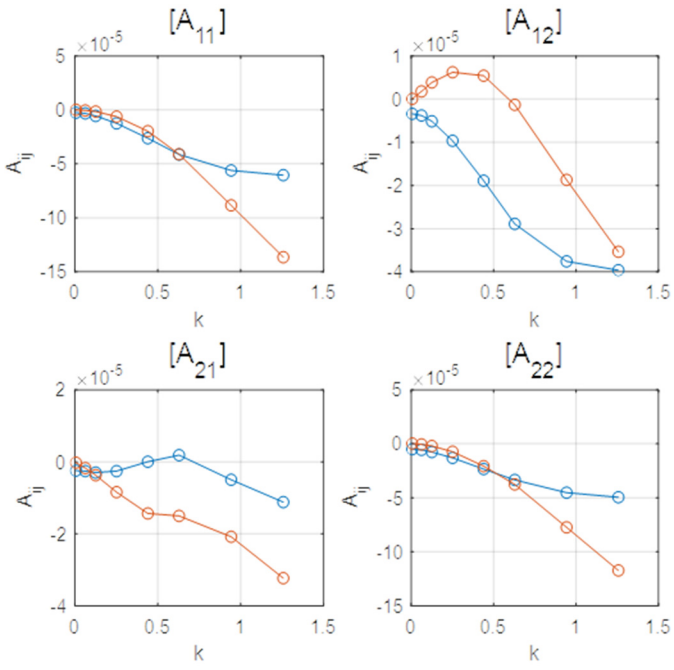


Figure 13 – UAIC $A_{11}$ to $A_{22}$

The frequency domain aeroelasticity stability analysis was performed with the V-g method and p-k method, using the UAIC calculated by the HOM. The analysis conditions were air density and dynamic pressure at an altitude of 11 km. Figures 14 shows the V-g method and p-k method results, respectively. The results showed that divergence occurred in the 1st bending mode at velocity of 3020 m/s. Since the result is a very high area that is more than 10 times of 300 m/s or less, it was confirmed that it is stable in the Mach number of 0.88 analyzed.

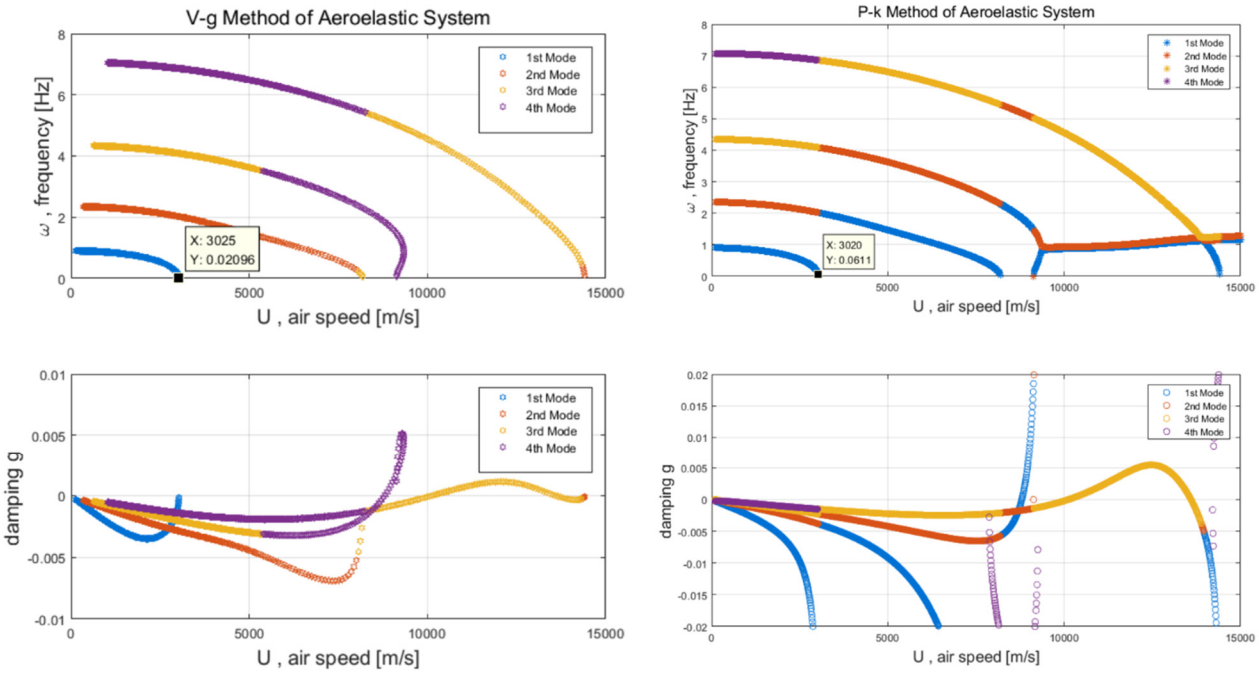


Figure 14 – V-f and V-g plot of V-g method (Left) / V-f and V-g plot of p-k method (Right)

### *3.2.3 Time Domain Analysis*

Through Kalpel's Minimum-States Approximation, the aeroelastic response in the time domain can be performed by the time integral of the aeroelastic equation in the form of a state space equation.

The time domain analysis calculates an aeroelastic response in the time domain with respect to one input speed. It takes a lot of computational resources to generate the response at all speeds, such as the frequency domain. Therefore, the analysis was performed on several cases near the predicted unstable point in the frequency domain analysis. The aeroelastic responses of the nose in the launch vehicle with different cases, i.e. 2500 m/s, 3000 m/s, 3030 m/s, are shown in Fig. 15. It is observed that the convergence was achieved for case 1, which is the stable area. When increasing the speed leading to a decrease in the frequency of vibration, it is predicted that an abrupt divergence between case 2 and case 3.

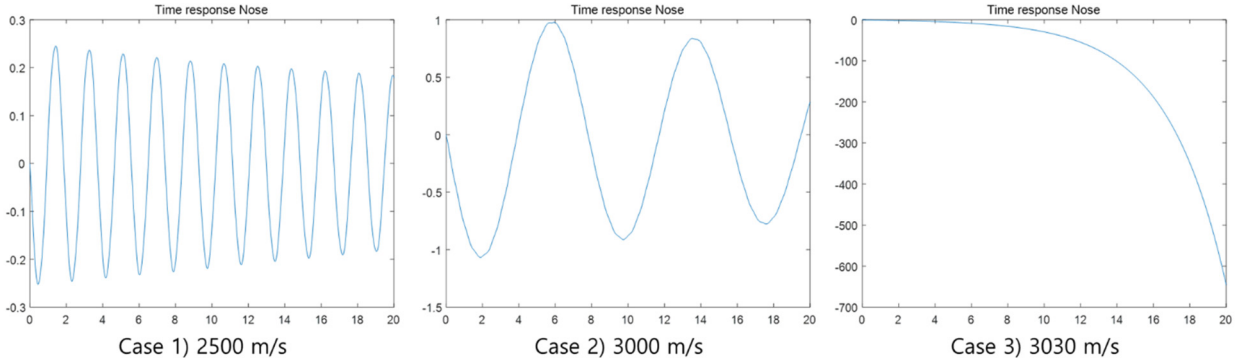


Figure 15 – Time history of aeroelastic response in three cases

### 3.2.4 CFD-CAE Coupled Method

The CFD-CAE coupled analysis was performed under the same conditions as frequency domain analysis and time domain analysis with unsteady aerodynamic force approximation. Similar to time domain analysis using aerodynamic approximation, CFD-CAE coupled method calculates an aeroelastic response for one input speed. The analysis was repeatedly carried out in the previously predicted speed range, and it was predicted that there was a divergence occurs at 3100 m/s. Figure 16 shows the displacement time history of the FEM nodes at the hammerhead pairing part, boattail part, and end part of the launch vehicle. From the direction and magnitude of the three parts, divergence occurs in a 1st banding mode shape.

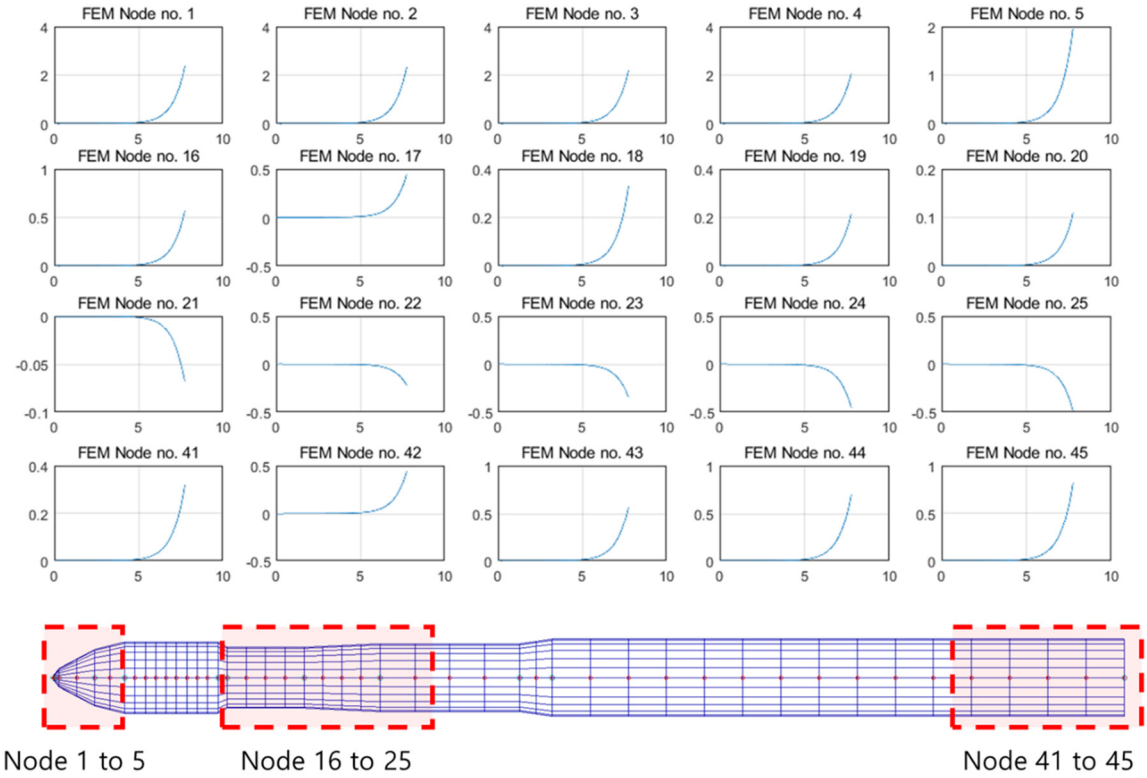


Figure 16 – Time history of the displacement at FEM nodes

### 3.2.5 Results

The results of the analysis using the UAIC calculated with HOM and the analysis using CFD-CAE coupled method are summarized and shown in a Table 2.

| | Frequency and Time domain analysis using UAIC with HOM | | | CFD-CAE coupled method |
|---|---|---|---|---|
| | V-g method | p-k method | Time-marching | |
| Divergence Speed (m/s) | 3025 | 3020 | 3030 | 3100 |
| Mode | 1st bending | 1st bending | 1st bending | 1st bending |

Table 2 – Aeroelastic analysis results of KSLV II model at M = 0.88

## 4. Conclusion

In this study, the aerodynamic instability that may occur in the transonic region of the hammerhead-type launch vehicle was analyzed using CFD-CAE coupled method. The in-house computational fluid analysis program KFLOW was used, and steady and unsteady flow analysis of the KFLOW was performed using Model 11 launch vehicle. The obtained result was verified with experimental data. The beam spline method for numerical interpolation between FEM model and CFD mesh, and the harmonic oscillation method for calculating the unsteady aerodynamic influence coefficients were used. The unsteady aerodynamic forces analysis and CFD-CAE coupled analysis programs were developed using these methods. The FEM model of the KSLV II model was constructed using the provided data, and aerodynamic analysis were performed using developed program. Aeroelasticity stability analysis was performed in two ways. The first method calculated the UAIC matrix using the harmonic method and substituted it in the aeroelastic equation to perform frequency domain analysis and time domain analysis using aerodynamic approximation. In the second method, time domain analysis was performed using CFD-CAE coupled method. It was carried out that the four analysis results calculated from the above methods were almost identical. The analysis FEM model was a model with sufficient stiffness and mass properties, so the divergence phenomenon was predicted at a very high speed. It leads to that if the stiffness of the launch vehicle structure model is insufficient, aeroelasticity instability can be occurs in the relevant operating region.

## 5. Acknowledgment

The authors gratefully acknowledge the financial support provided by ˙Agency for Defense Development under the contract UD210028JD and the contract TE210646JD.

## 6. Contact Author Email Address

mailto: jsbae@kau.ac.kr

## References

[1] R.V.J. Dogget and H.P. W., “An Aeroealstic Model Approach for the Prediction of Buffet Bending Loads on Launch Vehicles,” NASA Technical Note, NASA TN D-2022, 1963.

[2] M. Trikha, D.R. Mahapatra, S. Gopalakrishnan, R. Pandiyan, “Analysis of Aeroelastic Stability of a Slender Launch Vehicle using Aerodynamic Data,” 46th AIAA Aerospace Sciences Meeting, No. 310, 2008.

[3] L.E. Ericsson and D. Pavish, “Aeroelastic Vehicle Dynamics of a Proposed Delta II 7920-10L Launch Vehicle,” Jornal of Spacecraft and Rockets, Vol. 37, No. 1, 2000, pp. 28-38.

[4] R. Camussi, G. Guj, B. Imperatore, A. Pizzicaroli, D. Perigo, “Wall pressure fluctuations induced by transonic boundary layers on a launcher model,” Aerospace Science and Technology 11 (2007) 349–359

[5] A. G. Rainey, “Progress on the Launch-Vehicle Buffeting Problem,” Journal of Spacecraft and Rockets, Vol. 2, No. 3, 1965, pp.289-299.

[6] J.P. Reding, L.E. Ericsson, “Hammerhead Aeroelastic Stability Revisited,” AIAA-93-1477-CP.

[7] K.W. Dotson, R.L. Baker, B.H. Sako, “Self-sustained Oscillation of Launch Vehicles Caused by Aeroelastic Coupling,” 57th International Astronautical Congress, 2006, 10.2514/6.IAC-06-C2.7.11.

[8] K.W. Dotson, R.L. Baker, B.H. Sako, “Launch Vehicle Buffeting with Aeroelastic Coupling Effects,” Journal of Fluids and Structures, Vol. 14, 2000, pp. 1145-1171.

[9] K.W. Dotson, R.L. Baker, R.J. Bywater, “Launch Vehicle Self-sustained Oscillation From Aeroelastic Coupling Part 2 : Analysis, Jornal of Spacecraft and Rockets, Vol. 35, 1998, pp. 374-379.

[10] Dynamic Response of a Family of Axisymmetric Hammerhead Models to Unsteady Aerodynamic Loading. National aeronautics and space Administration, 1968.

[11] Hanson, Perry W., and Robert V. Doggett Jr. Aerodynamic damping and buffet response of an aeroelastic model of the Saturn I Block II launch vehicle. No. NASA-TN-D-2713. NATIONAL AERONAUTICS AND SPACE ADMINISTRATION HAMPTON VA LANGLEY RESEARCH CENTER, 1965.

[12] Hanson, Perry W., and Robert V. Doggett. Wind tunnel measurements of aerodynamic damping derivatives of a launch vehicle vibrating in free-free bending modes at Mach numbers from 0.70 to 2.87 and comparisons with theory. National Aeronautics and Space Administration, 1962.

[13] F. Mastroddi, F. Stella, G.M. Polli, M. Giangi, “Sensitivity Analysis for the Dynamic Aeroelasticity of a Launch Vehicle,” Journal of Spacecraft and Rockets, Vol. 45, No. 5, 2008, pp. 999-1009.

[14]R.E. Bartels, P. Chwalowfki, S.J. Massey, J. Heeg, C.D. Wieseman, R.E. Mineck, “Compuational Aeroelastic Analysis of the Ares I Crew, Launch Vehicle During Ascent,” Journal of Spacecraft and Rockets, Vol. 49, 2012, pp. 651-658.

[15]C.F. Coe, “The Effects of Some Variations in Launch-Vehicle Nose Shape on Steady and Fluctuating Pressures at Transonic Speeds,” NASA TM-646, March 1962.

[16]Caughey, D. A., "Diagonal Implicit Multigrid Algorithm for the Euler Equations," AIAA Journal, Vol. 26, No. 7, 1988, pp.841-851.